International Commission of Coal and Organic Petrology (ICCP)

Commission II Geological Applications of Organic Petrology

The Confocal Laser Scanning Microscopy Working Group of the ICCP: Final Report 2021

by Paul C. Hackley, U.S. Geological Survey, phackley@usgs.gov; Jolanta Kus, BGR, jolanta.kus@bgr.de; João Graciano Mendonça Filho, UFRJ, graciano@geologia.ufrj.br; Andrew D. Czaja, Univ. Cincinnati, czajaaw@ucmail.uc.edu; Angeles Borrego, INCAR, angeles.g.borrego@csic.es; Dragana Životić, Univ. Belgrade, dragana.zivotic@rgf.bg.ac.rs

Abstract

This report summarizes the activities and results of the Confocal Laser Scanning Microscopy (CLSM) working group (WG) of the International Committee for Coal and Organic Petrology (ICCP), from its inception in September, 2015, to the present day (September, 2021). The purpose of this report is to document the history of the working group and to compile and evaluate its results. The CLSM WG examined an immature, organic-rich sample of Kimmeridge Clay, which was characterized via CLSM imaging and spectroscopy. In addition, mechanically polished and broad ion beam (BIB) milled sample preparations were characterized via atomic force microscopy. Highlights of findings from the CLSM WG include: the interpreted presence of *Botryococcus*; incomplete blocking of laser light from highly reflective materials; surface roughening and surface flattening induced by differential BIB milling dependent on location and scale of measurement; substitution of uranium for iron in sulfides; red-shift of reflectance and auto-fluorescence from below the sample surface; positive alteration from laser-induced photo-oxidation of the sample surface including fluorescence blue-shift; blue-shift associated to higher fluorescence intensity regions in amorphous organic matter; need for fluorescence spectroscopy standardization as applied via CLSM; and the suitability of CLSM to predict solid bitumen reflectance via calibration to an extant data set. Due to the inability of WG members to continue participating in a WG format, the CLSM WG is hereby finalized. This report represents the final product of WG activity, with the aim to summarize the information included herein for a future peer-reviewed manuscript.

Introduction

The International Committee for Coal and Organic Petrology (ICCP) was founded in 1951 to formalize nomenclature for the petrographic constituents of coal and is constituted by working groups in which ICCP members collaborate to provide solutions for recalcitrant problems in organic petrology. An annual meeting is held in different locations every year, where the main proceedings consist of presentations and informal discussions held within the active working groups. As outlined on the ICCP website, https://www.iccop.org/about/, "working group activities and exercises are designed to resolve common problems and to establish uniform terminologies and analytical procedures for the microscopic investigation of organic materials in coals, oil shales and sedimentary rocks."

History of the Confocal Laser Scanning Microscopy Working Group (CLSM WG)

This report updates the status and activities of the Confocal Laser Scanning Microscopy Working Group (CLSM WG), which was established at the 2015 meeting of the ICCP held in Potsdam, Germany. The CLSM WG was established within Commission II of ICCP—Geological Applications of Organic Petrology—with the general objective to investigate applications of CLSM to organic petrology. Establishment of the WG followed a successful collaborative study by the conveners (Hackley and Kus) using CLSM as a thermal maturity probe of *Tasmanites* algal bodies [1, 2], and independent earlier and ongoing research by both conveners [3-6].

Following approval of the proposed WG at the Potsdam meeting, a call for participation was placed in *ICCP News* No. 63 (Nov. 2015, p. 33, https://www.iccop.org/publications/iccp-news/). Thereafter, a questionnaire was distributed via email in February, 2016, to test participant interest and instrument access, parameters of

the available instruments, and potential organic petrology applications that members of the WG would be inclined to test and investigate. Based on responses to this survey, and through further calls for participation in *ICCP News* and *The Society for Organic Petrology (TSOP) Newsletter* (https://www.tsop.org/newsletter.html), the initial participants in the WG were identified. Additional participants were recruited at the 2015 Geological Society of America meeting in Baltimore, Maryland, and at the joint 2016 meeting of ICCP-TSOP and the American Association for Stratigraphic Palynology (AASP) in Houston. Altogether, persons indicating their potential interest to participate included: Magdalena Misz-Kennan (University of Silesia, Poland), Isabel Suarez-Ruiz [Instituto Nacional del Carbón (INCAR), Spain], Katrin Ruckwied (Shell, USA), Mark Curtis (University of Oklahoma, USA), Stavros Kalaitzidis (University of Patras, Greece), John Firth (International Ocean Discovery Program-Texas A&M, USA), Ingrid Romero (University of Illinois, USA), Bill Schopf [University of California, Los Angeles (UCLA), USA], Ibrahim Al Atwah (Texas A&M, USA), Shibu Arens (AIM GeoAnalytics, USA), and the co-authors of this report, for a total of 16 participants.

The instruments potentially available to the participants included a Keyence VK-X200 series microscope (Univ. Oklahoma), Leica SP5 AOBS inverted (BGR), Leica SP2 inverted (Univ. Belgrade), Olympus FluoView FV300 (UCLA), Olympus FluoView 1000 (Univ. Cincinnati), and a Leica SP5 X (Univ. Maryland), among others. Participants indicated a diverse set of inclinations for CLSM application and their interest in multiple imaging applications: artificial fracture networks; proppant embedment; three-dimensional (3-D) characterization of sedimentary organic matter; sub-microscopic identification of sedimentary organic matter; 3-D distribution of oil inclusions; and cellular morphology. Further, participants were interested to test spectroscopy applications of CLSM, including characterization of sedimentary organic matter; use of CLSM as a thermal maturity probe; and spectroscopic relationships between sedimentary organic matter composition and structure.

An update for the WG was provided in *ICCP News* No. 66 (Dec. 2016, p. 24, https://www.iccop.org/publications/iccp-news/), announcing the intention of the WG "to function as a multi-year interlaboratory study, trading common perspectives and approaches within confocal laser scanning microscopy as applied to sedimentary organic matter and to organic petrology in general." Furthermore, it was suggested that "potential outcomes of the CLSM WG may include a 'white paper' reviewing techniques and applications, or a research paper(s) describing consensus objective(s) from an interlaboratory study."

Leading up to the 2017 ICCP meeting in Bucharest, Romania, members of the WG investigated potential samples for an interlaboratory study (ILS), ultimately deciding on a Kimmeridge Clay Formation oil shale sample, which was being used for several ongoing U.S. Geological Survey (USGS) studies [7-10]. The overall abundance of bituminite was the primary reason for selection of this sample as the object of study. The decision to investigate this sample in the CLSM WG was formally confirmed at the 2017 ICCP meeting. Following the 2017 meeting, Stavros Kalaitzidis (Univ. Patras, Greece) established an ICCP webpage for the CLSM WG, which can be accessed from: https://www.iccop.org/workinggroup/confocal-laser-scanning-microscopy-clsm/. The webpage provides identities of the WG conveners and their contact information, as well as a list of the WG participants. A short description of the WG objectives and activities also was included.

The Kimmeridge Clay Formation (sample ID: KC-1) sample was sent from the USGS to the laboratory of João Graciano Mendonça Filho at the Federal University of Rio de Janeiro in Brazil, where it was processed for preparation of kerogen strew slides, and as a kerogen concentrate finished into polished pellets. Sample materials were returned to the USGS, from which the raw material and various preparations (polished whole rock plug, polished kerogen concentrate, strew slide of kerogen concentrate) were distributed in April, 2018, to 13 of the original WG participants. Several initial members of the WG had, by this time, changed employment or dropped participation for other reasons. During 2018, several WG members made initial progress in CLSM analysis of the KC-1 sample (detailed characterization below), and these results were compiled and presented in a summary format for the 2018 ICCP meeting in Brisbane, Australia.

CLSM data was contributed from an additional member of the WG in 2019, but discussion at the 2019 ICCP meeting in The Hague centered on how to rejuvenate WG activities, which had waned, and how to solicit

further contributions from the participants. The global COVID-19 pandemic prevented any WG progress in 2020, during which the ICCP meeting was altogether cancelled.

Beginning in March, 2021, during the continued global COVID-19 pandemic, and under mandated work-from-home conditions and continued travel restrictions, the CLSM WG conveners started meeting via approximately monthly videoconferences to discuss status, progress, and potential resolutions of the CLSM WG. That interaction led to several outcomes, including: 1) the compilation of this report, 2) a note to update the activities of the WG in *ICCP News* No. 79 (May, 2021, p. 5), 3) an update to the ICCP CLSM WG webpage https://www.iccop.org/workinggroup/confocal-laser-scanning-microscopy-clsm/, 4) cross-linking of the WG conveners' respective project webpages https://www.robeha.de/EN/Themen/Energie/Projekte/laufend/CLSM_en.html?nn=1548120 (Kus) and https://www.usgs.gov/centers/gemsc/science/thermal-indices-innovation (Hackley), 5) joint initial development of a CLSM review paper for applications in organic petrology, 6) sample exchange to extend prior collaborative work [1], and 7) new sample exchange to investigate fluid inclusions via CLSM in an Upper Cretaceous petroleum system in the onshore Gulf of Mexico Basin of the USA [11].

In April, 2021, the 13 members of the CLSM WG who had received the KC-1 sample were contacted with a request to contribute final results. CLSM WG members were also asked to return to the conveners any remaining materials of whole rock mount, kerogen concentrate, or strew slide. WG members were asked if they were still interested in the activities of the WG or wished to participate in the future. Two members of the WG replied to indicate they could no longer participate in activities; no reply was received from the others, which was interpreted to mean they could not participate further. Based on this outcome, the conveners decided to close and finalize the activities of the CLSM WG and revert to a collaborative relationship. The history of the CLSM WG is summarized in Table 1.

Table 1. Summary by year of CLSM WG activities.

Year	Activities
2015	Confocal laser scanning microscopy (CLSM) working group (WG) established at Potsdam ICCP meeting; participants recruited at Baltimore, Maryland (USA) Geological Society of America meeting
2016	Questionnaire distributed to participants; participants recruited at Houston ICCP meeting
2017	Kimmeridge Clay (KC) sample selected as CLSM target; CLSM WG webpage established
2018	KC sample processed and distributed; CLSM data collection by contributors summarized at Brisbane ICCP meeting
2019	Discussion to rejuvenate activities of CLSM WG at The Hague ICCP meeting
2020	Global COVID-19 pandemic; ICCP meeting cancelled; no progress in CLSM WG
2021	CLSM WG finalized; final report prepared

Characterization of Kimmeridge sample used by the CLSM WG

The Kimmeridge Clay Formation sample used by the CLSM WG was collected (by Michael Lewan, USGS Emeritus) from the Blackstone oil shale layer outcropping on the Dorset coast of southern England in the Wessex Basin (coordinates 50.5975, -2.0930), near the town of Kimmeridge between Kimmeridge Bay and Chapmans Pool. The sample contains approximately 44 weight percent total organic carbon content [7] and is mostly comprised of fluorescent amorphous organic matter (AOM), which is also called bituminite [12] (**Fig. 1A**). Bituminite has a reddish tint (in incident white light; **Fig. 1B**) and lacks a gray reflecting surface after typical petrographic polish to a finish of 0.05 µm. Dispersed terrigenous inertinite is common and vitrinite is present in trace amounts (**Fig. 1B**). Scattered sporinite and discrete telalginite bodies are sparse. Some micrinite is present (**Fig. 1B**) from early conversion of the bituminite [13], or due to diffuse light scattering from dispersed clay minerals [14]. Radiation alteration halos are present as zones of red-shifted and diminished fluorescence

intensity surrounding heavy minerals(?) and sulfides embedded in the AOM (**Fig. 1A**). Although radiolytic damage to sedimentary organic matter usually causes an increase of organic reflectance, e.g., [15, 16], this effect was not observed in the bituminite of the KC-1 sample. Mean reflectance of scarce solid bitumen is 0.29% (s.d.=0.03, n=13, [7]), whereas mean vitrinite reflectance is 0.42% (s.d.=0.03, n=13). Mean reflectance of the AOM is 0.16% (s.d.=0.02, n=55, [8]). A white to red (in incident white light; **Fig. 1D**) sulfide and its weathering products occur as framboids, replacing shell (fossilized bone?), and the weathering products (goethite plus carbonate?) show long wavelength fluorescence. Unaltered pyrite framboids also are common.

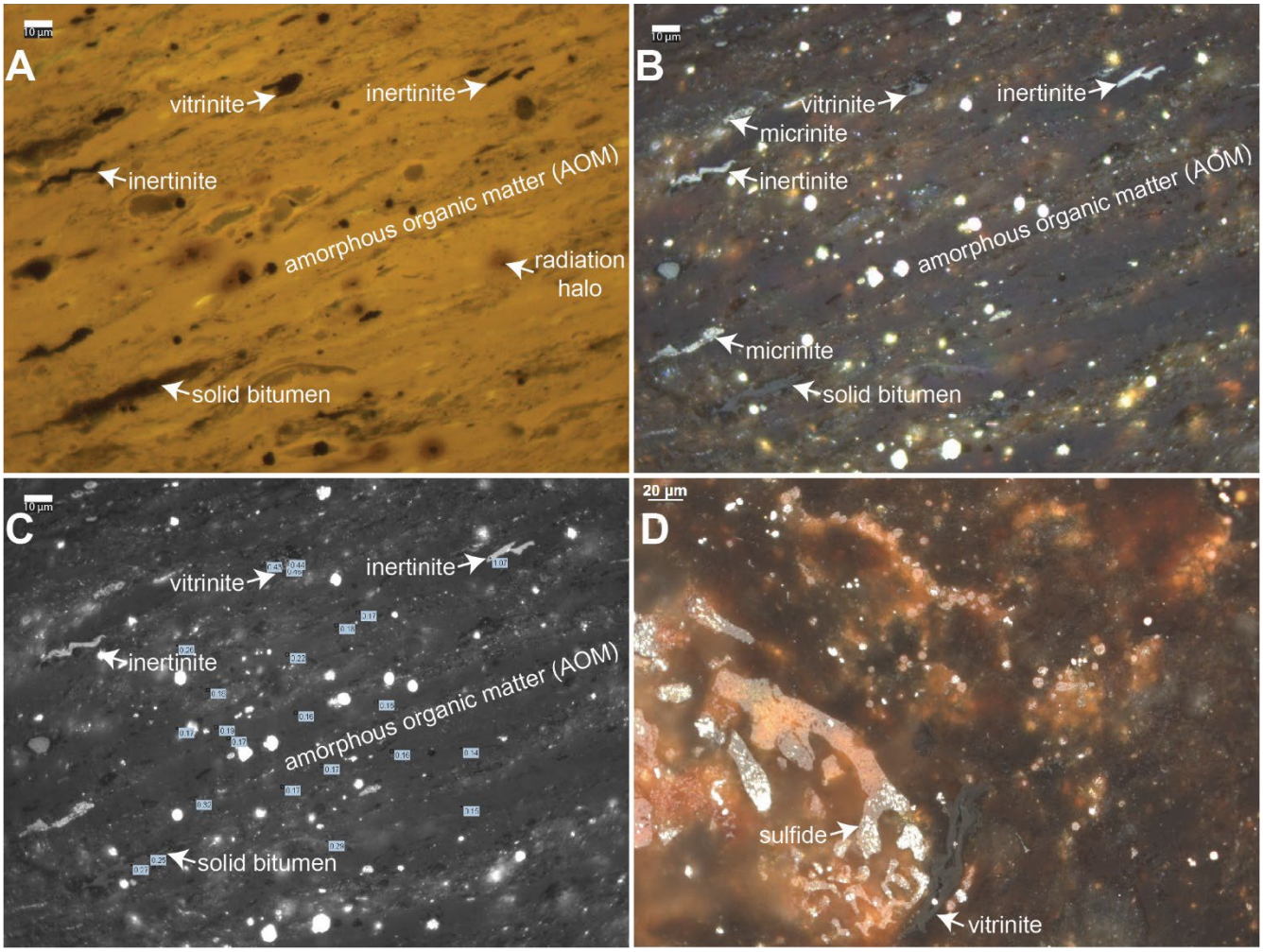

Figure 1. Optical photomicrographs of the KC-1 sample selected for study in the CLSM WG. **A**. Bituminite (labeled as amorphous organic matter (AOM) in epi-fluorescence (under oil immersion) showing scattered terrigenous macerals (vitrinite and inertinite) and radiation halos (decreased fluorescence intensity emission areas with color red-shift) around heavy minerals and sulfides. **B**. Same field as A under incident white light. **C**. Same field as A-B taken with a monochrome camera showing reflectance values of selected measurement areas. **D**. Sulfide altering to oxidation products and replacing bone(?) under incident white light and oil immersion.

The bituminite in the KC-1 sample shows a substantial increase in reflectance following broad ion beam (BIB) milling sample preparation, which was investigated via atomic force microscopy (AFM) [8]. As shown in **Figure 2A-D**, a selected region of AOM increased in mean reflectance from 0.18% (s.d.=0.02, n=100, **Fig. 2A**) to 0.38% (s.d.=0.03, n=100, **Fig. 2C**) after gentle BIB milling in a Hitachi IM 4000 Plus ion mill for 5 min, using 4 keV, 15° incline, 360° rotation at 25 rpm, and 100% focus (1.5 kV discharge; ~100 µA). The increase in reflectance by 0.20% (absolute) was accompanied by a substantial decrease in aerial root-mean-square surface

roughness (S_q, root-mean- square value of the ordinate values of the surface height distribution [17, 18], where lower values indicate flatter surfaces) as determined via AFM.

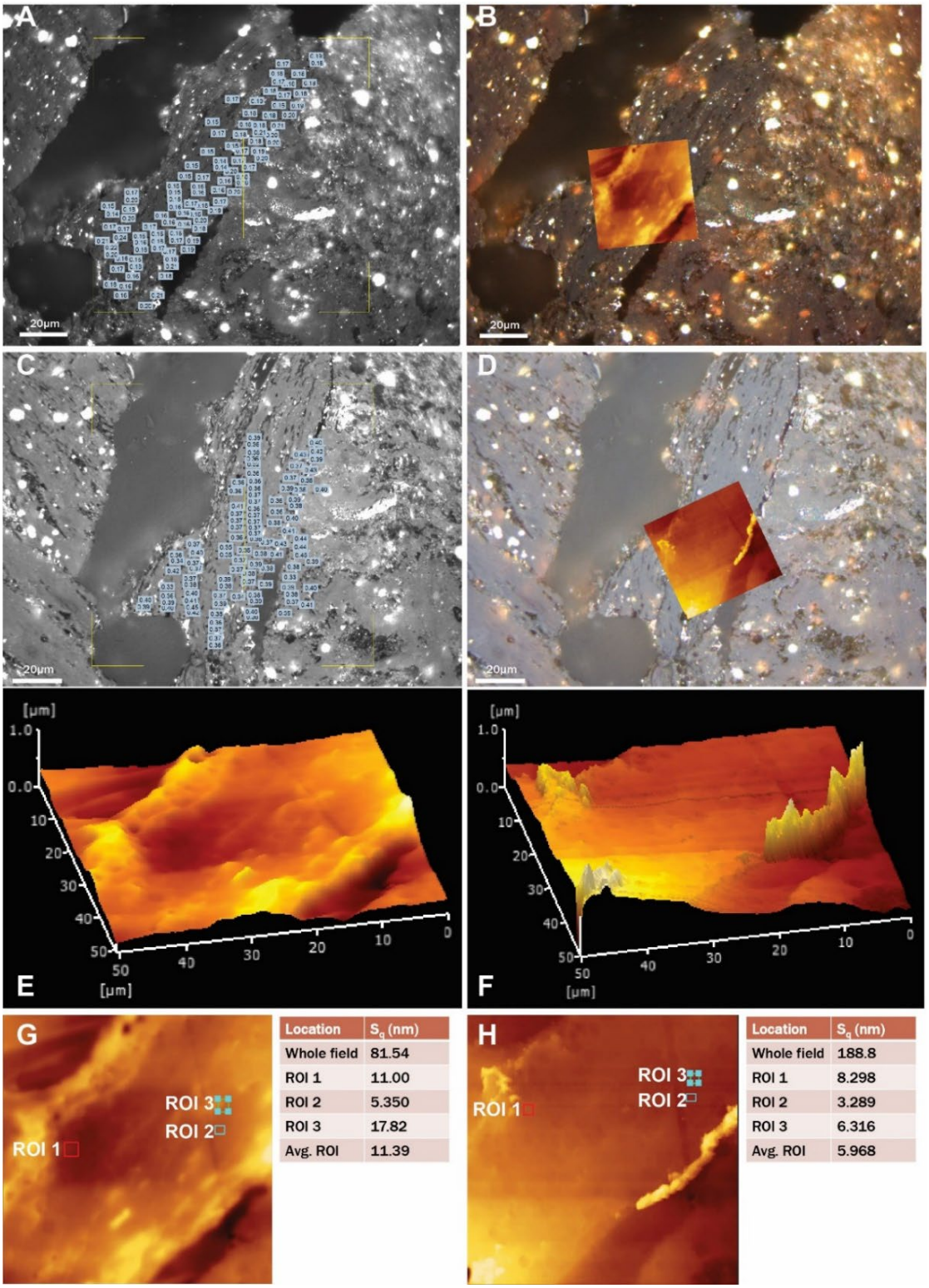

Location	S_q (nm)
Whole field	81.54
ROI 1	11.00
ROI 2	5.350
ROI 3	17.82
Avg. ROI	11.39

Location	S_q (nm)
Whole field	188.8
ROI 1	8.298
ROI 2	3.289
ROI 3	6.316
Avg. ROI	5.968

Figure 2. Reflectance increase and surface flattening of amorphous organic matter (AOM) in the mechanically polished KC-1 sample caused by broad ion beam (BIB) milling. **A**. Reflectance of mechanically polished AOM pre-BIB milling, monochrome. **B**. Same field as A with atomic force microscopy (AFM) overlay, color. **C**. Reflectance of AOM post-BIB milling, monochrome. **D**. Same field as C with AFM overlay, color. **E**. 3-D representation of AFM topology, pre-BIB milling.

F. 3D representation of AFM topology, post-BIB milling. **G**. AFM topology pre-BIB milling showing three regions of interest (ROI) in AOM and the corresponding S_q values. **H**. AFM topology post-BIB milling showing three ROIs in AOM and corresponding S_q values.

Areas of AFM topology data collection before (**Fig. 2B**) and after (**Fig. 2D**) BIB milling are shown as colored squares located over ostensibly the same location of AOM. Note the development of a gray reflecting surface in the AOM in **Figure 2D**, similar to the appearance of solid bitumen [7]. The regions of AFM data collection are shown as 3-D representations in **Figure 2E-F**. A ridge formed by the relative polishing relief of quartz to the adjacent AOM is apparent post-milling near the right side of the 3-D image (**Fig. 2F**), showing that the softer AOM is preferentially removed by BIB milling. The relative milling relief between AOM and quartz results in an overall increase in S_q after milling, which is documented in **Figure 2G-H**, where S_q increases from approximately 82 to 189 nm during milling. However, as highlighted by the three regions of interest (ROI) in **Figure 2G-H**, the AOM experienced a relative decrease in S_q caused by the BIB milling, on average, from approximately 11 to 6 nm. The decrease in AOM surface roughness is interpreted to cause its increased reflectance post-milling, as described in previous works [7, 8, 19, 20].

A separate, non-correlative AFM investigation of the KC-1 sample showed overall increases in S_q *after* BIB milling. In this line of investigation, BIB milling of a mechanically polished sample surface used an E.A. Fischione 1060 SEM Mill (with broad beam conditions of 6 keV, 2° gun angle, 175° rotation at 3 rpm, 50% focus, 30 min). AFM data collection was on non-correlative locations, that is, two samples were used: 1) mechanically polished (to 0.05 µm) KC-1, and 2) mechanically polished (to 0.05 µm) and then BIB-milled KC-1. In the preceding discussion, the AFM analysis was on a correlative location in the same KC-1 sample before and after BIB milling (**Fig. 2**). In the following discussion, the collection of AFM data was on non-correlative locations of AOM in different samples (**Figs. 3-5**).

The sample with only a mechanically polished surface (**Fig. 3A-E**) showed overall S_q values of 22 nm (20×20 µm field, **Fig. 3A**). Phase imaging of the same field (**Fig. 3B**) generally corresponds to the topographic image (**Fig. 3A**), suggesting a relatively homogeneous surface in terms of its mechanical properties (e.g., adhesion, stiffness, friction). This is further visualized in **Figure 3C** where the phase image is laid over the topography in a 3-D view, showing that topographic depressions correspond to negative phase shifts. Scratches from the mechanical polish are apparent in the overlay, particularly in the lower half of the image. Sub-micron-sized sulfides (nano-sulfides) are present as finely disseminated inclusions in AOM which polish out in relief (**Fig. 3A-C**). When progressively smaller and more homogeneous regions were selected for analysis on the mechanically polished surface, even lower values of S_q were realized. For three 3×3 µm homogeneous ROIs selected within the 20×20 µm field, S_q values of 4-8 nm were measured (**Fig. 3E**). The trend of lower S_q values from smaller fields continues at another location in the mechanically polished sample (**Fig. 4A-E**). **Figure 4A** shows an overall S_q of 9.6 nm for a 6.25×6.25 µm field, and still lower values of 1.80-2.44 nm for 950×950 nm ROIs (**Fig. 4E**). Phase imaging (**Fig. 4B**) again corresponds to topography (**Fig. 4C**), indicating homogeneity in mechanical properties of the surface.

The non-correlative KC-1 sample surface that was mechanically polished then BIB-milled showed higher S_q values of 121 nm (70×70 µm field, **Fig. 5**), 108 nm (50×50 µm field, **Fig. 6**), and 136 nm (12×12 µm field, **Fig. 7A-D**). Compared to surfaces that have only been mechanically polished (**Figs. 3-4**), **Figure 7A** shows ion-induced exposure of disseminated nano-sulfides in the sample surface and a much wider expression of phase shift (**Fig. 7B**). The wider expression of phase shift is due to the increased exposure of nano-sulfides (which have a positive phase shift relative to the bituminite). Scratches from mechanical polish are no longer apparent; instead curtaining effects are present as aligned troughs in bituminite. Similar to the mechanically polished surface (**Figs. 3-4**), smaller homogeneous ROIs of 1.5×1.5 µm within the 12×12 µm field showed lower S_q values of 10.7-16.8 nm (**Fig. 7E**), indicating that the measurement of surface roughness for petrographic preparations of the KC-1 sample is strongly dependent on the scale of observation, whether in mechanically polished or ion-milled surfaces. The smaller (1.5×1.5 µm) ROIs are, however, an order of magnitude rougher than similar-sized

areas in the mechanically polished surface. This increase in surface roughness (increase in S_q) after BIB-milling (with the Fischione mill and its corresponding milling conditions) is interpreted to reflect the relief created by differential milling and removal of the bituminite compared to its embedded nano-sulfide inclusions. We hypothesize this was caused by ion erosion of the softer bituminite, exposing the embedded nano-sulfides and thus creating relief measured as higher S_q values. An identical effect was described above in the correlative AFM investigation for preferential removal of bituminite relative to quartz, illustrated as a quartz ridge in **Fig. 2D, F, and H**, and a higher S_q value in the post-milled whole field area of data collection.

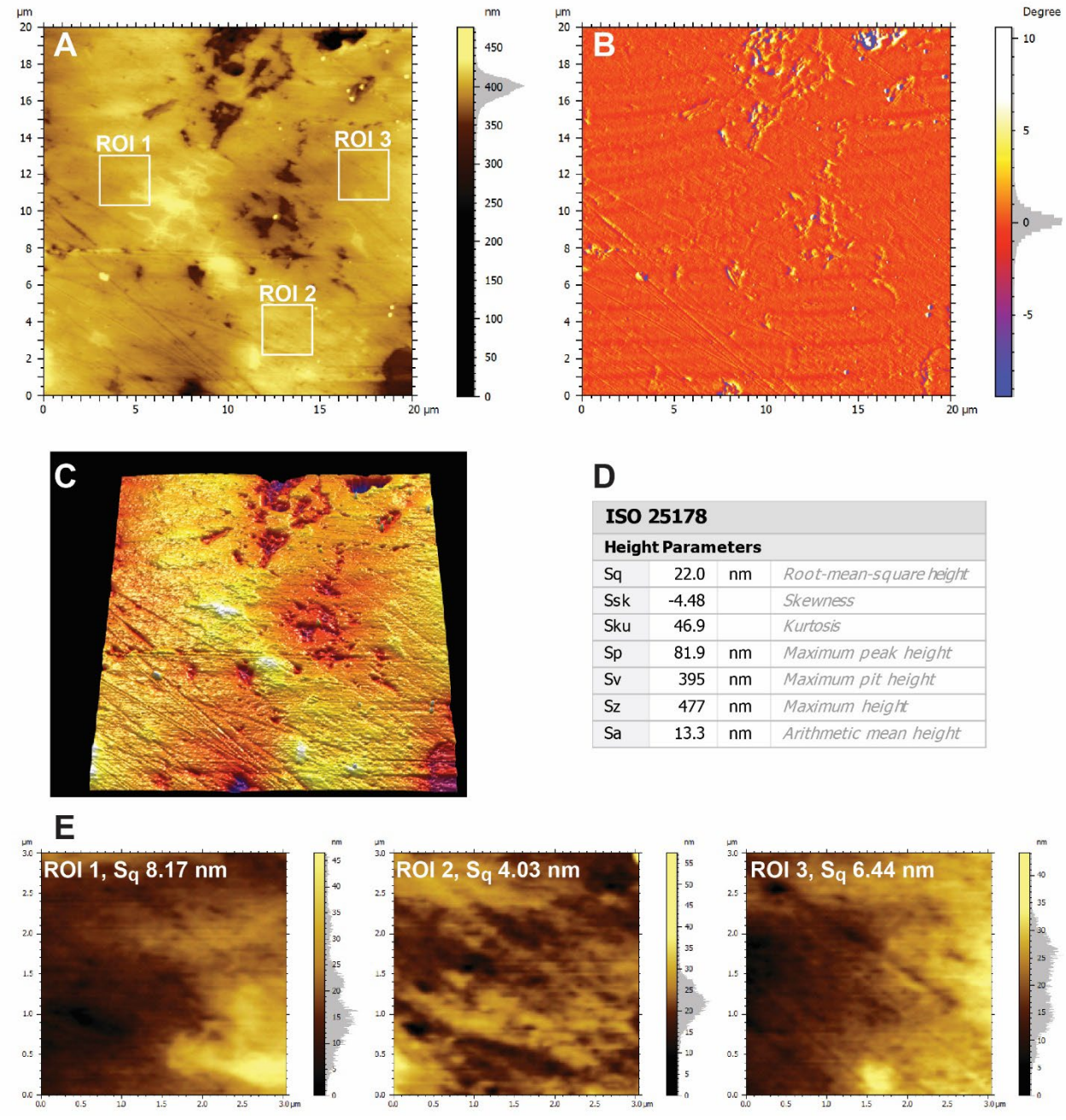

Figure 3. Atomic force microscopy (AFM) data from amorphous organic matter in mechanically polished KC-1 sample. **A**. AFM topography of 20×20 µm field. **B**. AFM phase contrast of same field as A. **C**. Phase contrast overlaid on 3D topology. **D**. Surface parameters. **E**. AFM topography from three 3×3 µm regions of interest (ROI) shown in A.

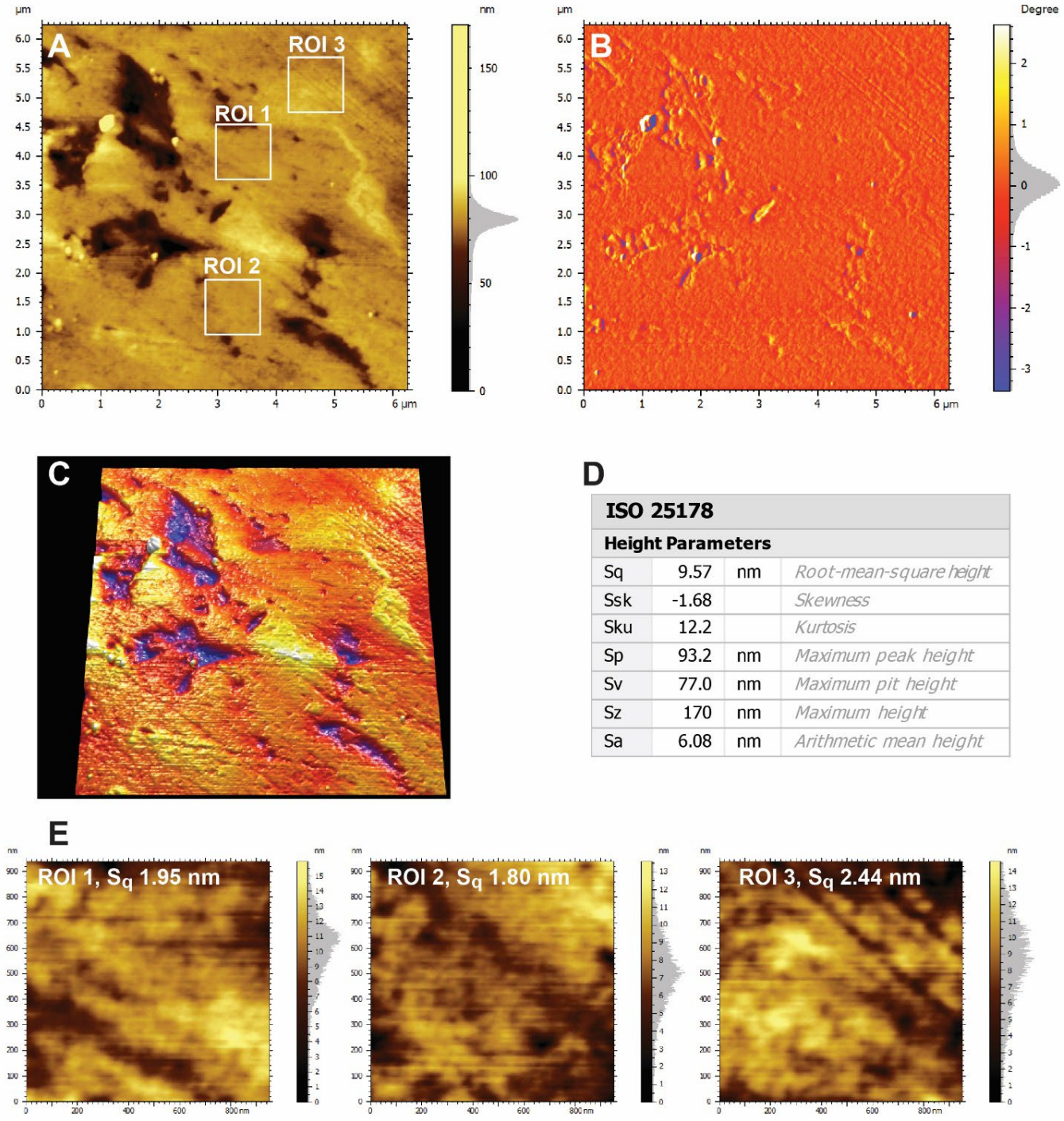

ISO 25178			
Height Parameters			
Sq	9.57	nm	*Root-mean-square height*
Ssk	-1.68		*Skewness*
Sku	12.2		*Kurtosis*
Sp	93.2	nm	*Maximum peak height*
Sv	77.0	nm	*Maximum pit height*
Sz	170	nm	*Maximum height*
Sa	6.08	nm	*Arithmetic mean height*

Figure 4. Atomic force microscopy (AFM) data from amorphous organic matter in mechanically polished KC-1 sample. **A**. AFM topography of 6.25×6.25 µm field. **B**. AFM phase contrast of same field as A. **C**. Phase contrast overlaid on 3D topology. **D**. Surface parameters for 6.25×6.25 µm field. **E**. AFM topography from three 950×950 nm regions of interest (ROI) shown in A.

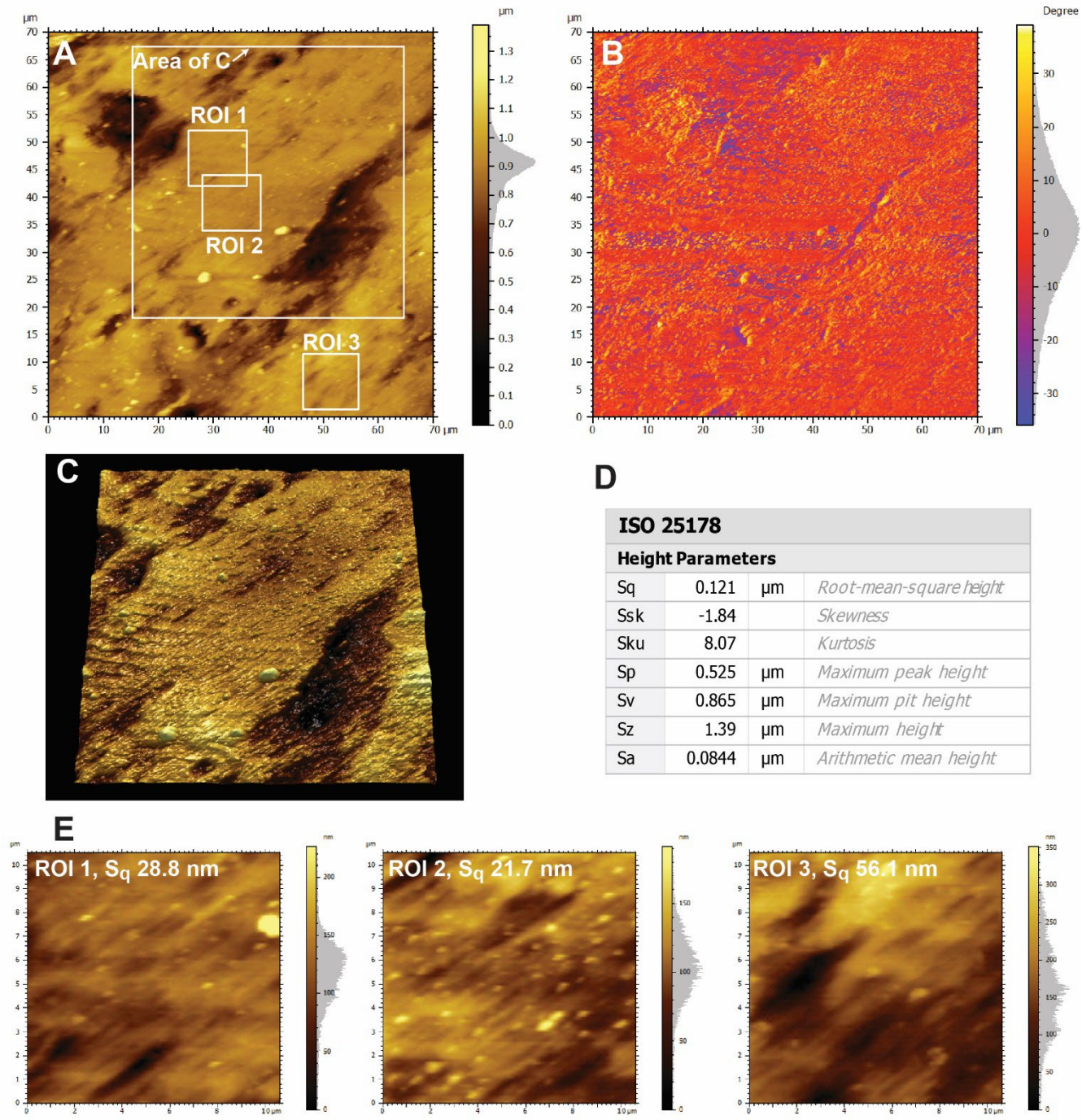

ISO 25178			
Height Parameters			
Sq	0.121	µm	*Root-mean-square height*
Ssk	-1.84		*Skewness*
Sku	8.07		*Kurtosis*
Sp	0.525	µm	*Maximum peak height*
Sv	0.865	µm	*Maximum pit height*
Sz	1.39	µm	*Maximum height*
Sa	0.0844	µm	*Arithmetic mean height*

Figure 5. Atomic force microscopy (AFM) data from amorphous organic matter in mechanically polished, then broad ion beam-milled KC-1 sample. **A**. AFM topography of 70×70 µm field. **B**. AFM phase contrast of same field as A. **C**. Phase contrast overlaid on portion of 3D topology. **D**. Surface parameters for A. **E**. AFM topography from three 10.6×10.6 µm regions of interest (ROI) shown in A.

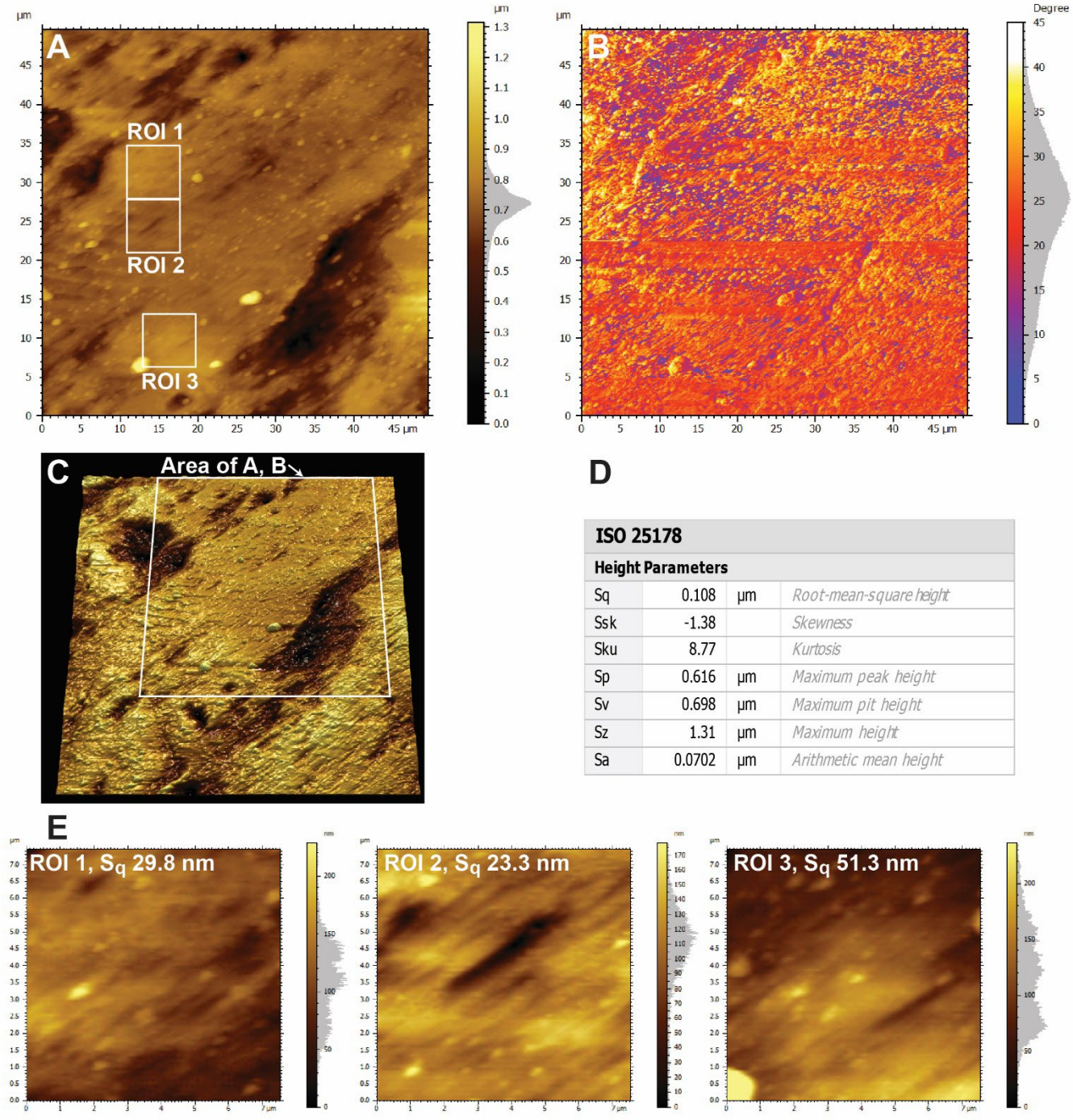

Figure 6. Atomic force microscopy (AFM) data from amorphous organic matter in mechanically polished, then broad ion beam-milled KC-1 sample. **A**. AFM topography of 50×50 µm field. **B**. AFM phase contrast of same field as A. **C**. Phase contrast overlaid on 3D topology (greater area than A-B). **D**. Surface parameters for A. **E**. AFM topography from three 7.5×7.5 µm regions of interest (ROI) shown in A.

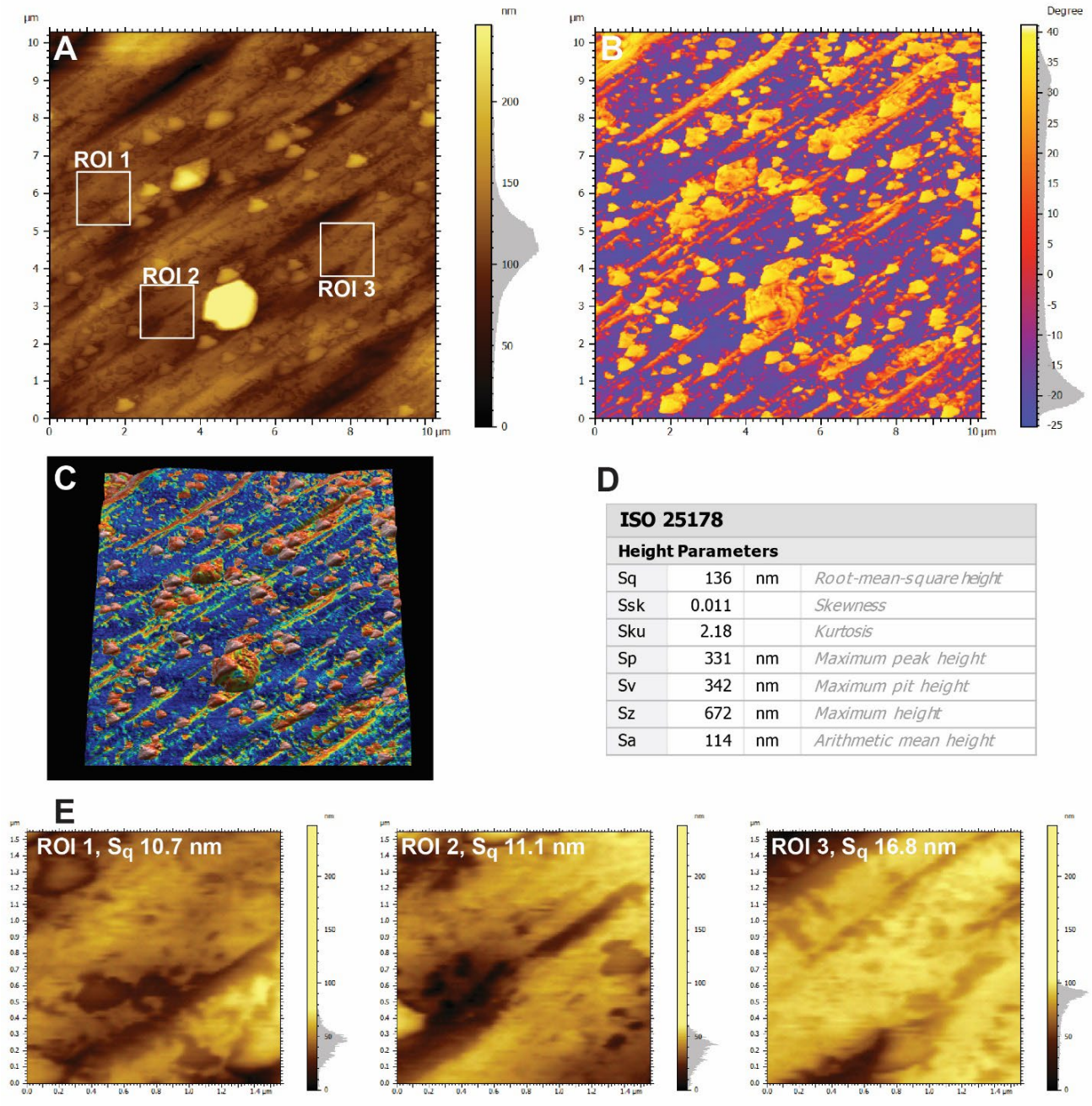

Figure 7. Atomic force microscopy (AFM) data from amorphous organic matter in mechanically polished, then broad ion beam-milled KC-1 sample. **A**. AFM topography of 12×12 µm field. **B**. AFM phase contrast of same field as A. **C**. Phase contrast overlaid on 3D topology. **D**. Surface parameters for 12×12 µm field. **E**. AFM topography from three 1.5×1.5 µm regions of interest (ROI) shown in A.

The act of mechanically polishing bituminite may 'smear' the soft organic matter over and around harder, embedded nano-sulfides, disguising their presence and reducing measured relief in the mechanically polished surface. Because the work using the Fischione mill was a non-correlative investigation (the same location was not investigated before and after BIB-milling), it is also possible that the consistently higher values of S_q in the milled sample may reflect locational differences in the material analyzed between the milled and non-milled samples. Nevertheless, the contradictory results between the correlative (lower S_q after BIB milling) and non-correlative (higher S_q after BIB milling) AFM investigations highlight our still limited understanding of the effects

of BIB milling to sedimentary organic matter [20], and show the need for further research before BIB milling can be advanced as a standard practice in sample preparation of sedimentary organic matter.

Results from CLSM investigation

The progress of WG members in CLSM analysis of the KC-1 sample was most substantial in 2018, and these results were compiled and presented in summary format for the 2018 meeting of the ICCP in Brisbane, Australia. The results are collated and further discussed in the following paragraphs.

CLSM imaging by Andrew Czaja (Univ. Cincinnati) is compiled in **Figure 8**, where the groundmass formed dominantly of bituminite hosts multiple other macerals and minerals. CLSM imaging was completed on an Olympus FluoView 1000 confocal system with a 60× oil immersion objective [1.42 numerical aperture (NA)], at 1024×1024 pixel resolution using a sampling speed of 40 µs/pixel and 4× digital zoom.

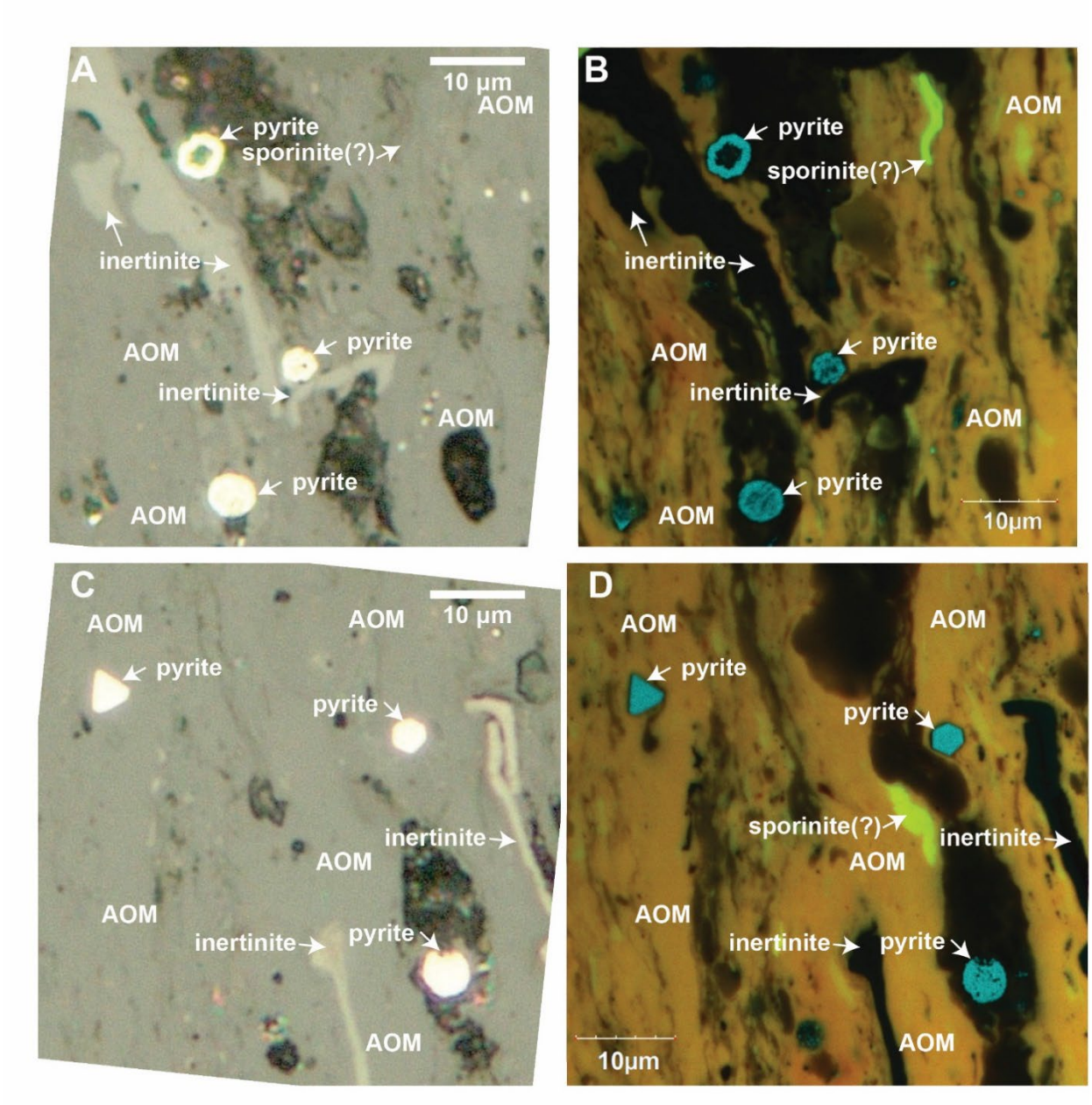

Figure 8. Optical and three-channel false color confocal laser scanning microscopy (CLSM) photomicrographs of KC-1 sample from CLSM WG participant Andrew Czaja (Univ. Cinn.). **A**. Optical image (dry 50× long working distance objective) showing amorphous organic matter (AOM), pyrite, inertinite, and sporinite(?). **B**. Same field as A imaged via CLSM showing yellow fluorescence of AOM, green fluorescence of sporinite(?), and blue laser (458 nm) reflection from pyrite. **C**. Optical image (dry objective) showing AOM, pyrite, inertinite, and sporinite(?). **D**. Same field as C imaged via CLSM showing yellow fluorescence of AOM, green fluorescence of sporinite(?), and blue laser reflection from pyrite. Note inability to differentiate sporinite(?) from AOM in optical images A and C and the fluorescence color contrast of sporinite/AOM in CLSM images B and D. Maceral identifications are interpreted by Hackley.

An important observation in the imaging by Czaja is the distinction in fluorescence color and emission intensity between terrigenous sporinite(?) (green, high intensity) and adjacent marine AOM (yellow, lower intensity). Radiation halos are present in both CLSM images (**Fig. 8B, D**), as indicated by a decrease in bituminite fluorescence intensity and red-shift, the same as noted in conventional fluorescence imaging (**Fig. 1A**). Also of note in the Czaja images is the Ar laser (458 nm) reflection from pyrite using a 480-495 bandpass filter (**Fig. 8B, D**). Each CLSM image is a three-channel composite as shown in **Figure 9**; the blue color of pyrite appears to be due to incomplete blocking of 458 nm reflected laser light by the 480-495 nm bandpass filter in the cyan channel.

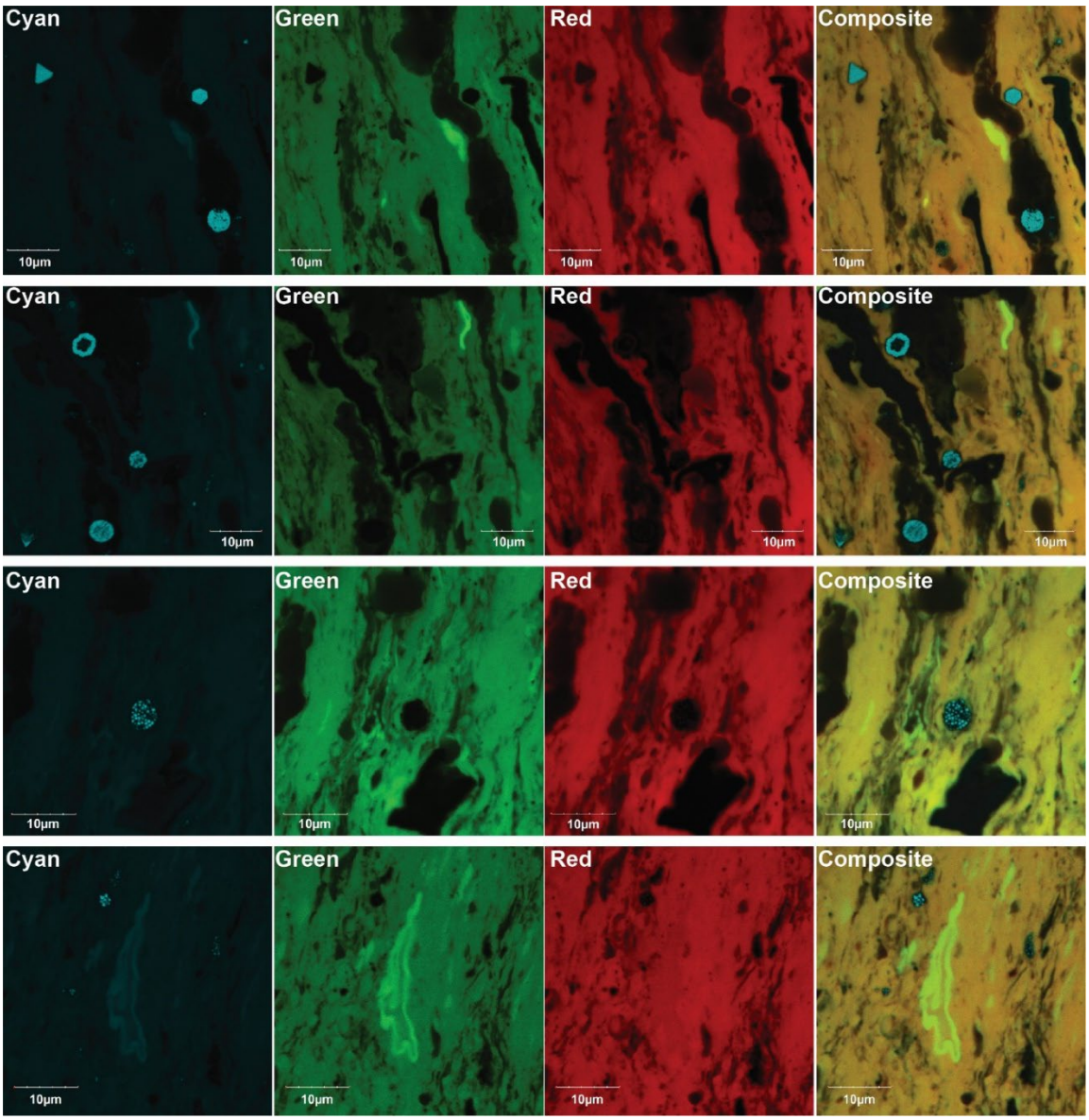

Figure 9. Three-channel construction of confocal laser scanning microscopy (CLSM) false color fluorescence composite images of KC-1 sample from CLSM WG participant Andrew Czaja. Cyan: 458 nm Ar laser, 480-495 bandpass filter. Green: 458 nm Ar laser, 535-565 bandpass filter. Red: 635 nm diode laser, 655-755 bandpass filter.

CLSM imaging by Jolanta Kus (BGR) was completed as part of official duties on a Leica TCS SP5 AOBS confocal system with a 63× oil immersion objective (1.4 NA), at 1024×1024 pixel resolution using a scan speed of 10Hz and a variable digital zoom. The applied laser lines were 458 nm, 496 nm and 633 nm. The emission bandwidth was from 455-492 nm, 499-629 nm, and 636-800 nm. Each of the CLSM images represent a composite image of false fluorescence color.

The imaging revealed a similar maceral assemblage as remarked above: bituminite (**Fig. 10A-D**), telalginite (**Fig. 10A, C**), inertinite (fusinite, **Fig. 10B**), and sporinite (**Fig. 10A, C**). As noted from conventional fluorescence microscopy, radiation halos occurring around blue-reflecting sulfide (noted by a decrease in fluorescence emission intensity and red-shift, **Fig. 10B, D**), or its oxidized replacement, may suggest some U substitution for Fe. Reflection of the blue laser line from highly reflective sulfides, as interpreted from the Czaja images (**Fig. 8B, D; Fig. 9**), is confirmed in images from Kus, which also show blue laser reflection from highly reflective fusinite with distinct 'bogen' [21] structure (**Fig. 10B**).

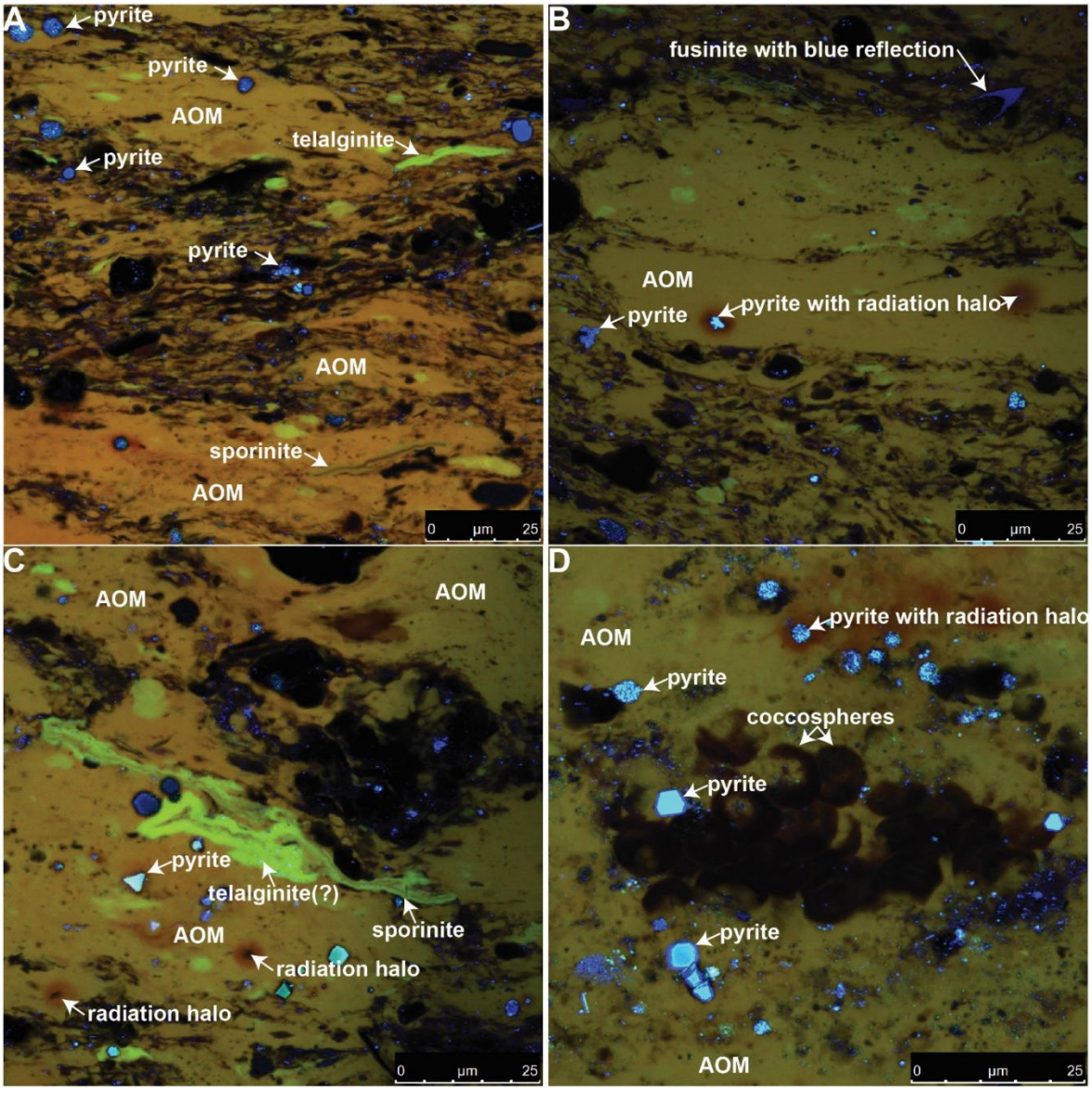

Figure 10. Three-channel construction of confocal laser scanning microscopy (CLSM) false color fluorescence composite photomicrographs of KC-1 sample from CLSM WG co-convener Jolanta Kus. **A**. Amorphous organic matter (AOM) with inclusions of pyrite, telalginite, and sporinite. **B**. AOM with 'bogen' structure fusinite. **C**. AOM with inclusions of pyrite, telalginite, and sporinite. **D**. AOM with coccosphere and pyrite inclusions. CLSM images captured with oil objective 63× and 1.40 NA by application of Ar and HeNe-lasers (excitation with 458 nm, 496 nm and 633 nm laser lines; voxel-width: A: 114.1 nm; B: 101.7 nm; C: 90.6 nm; D: 75.4 nm; scan format 1024×1024 pixel; digital zoom at 2.4, bidirectional scanning).

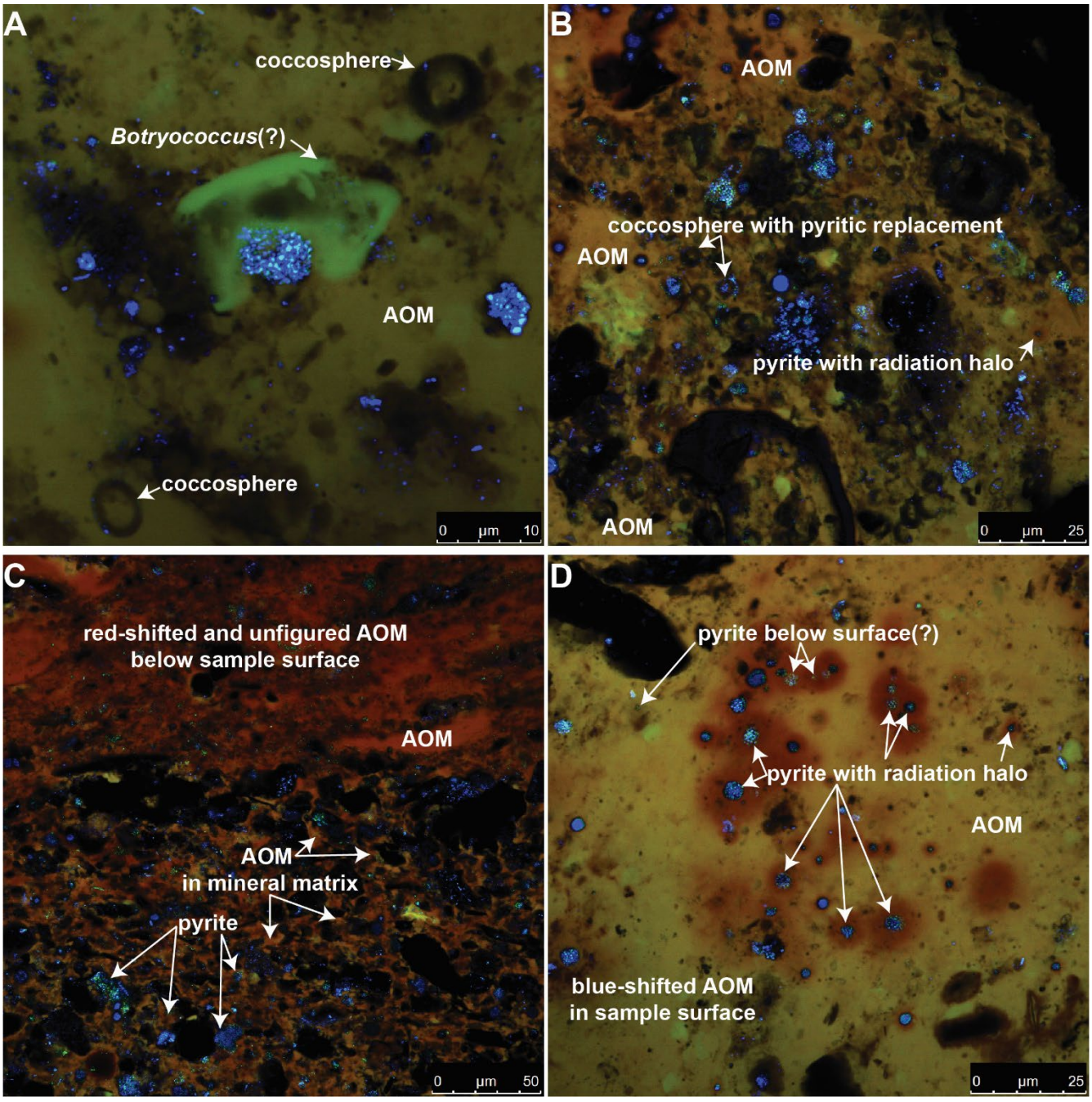

Figure 11. Confocal laser scanning microscopy (CLSM) photomicrographs of KC-1 sample from CLSM WG co-convener Jolanta Kus. **A**. *Botryococcus(?)* freshwater alga and coccospheres in amorphous organic matter (AOM). **B**. Coccospheres (some with pyritic replacement) in AOM. **C**. Red-shifted fluorescence of AOM and reflection from pyrite approximately 1.5 µm below the sample surface. **D**. Radiation halos surrounding blue-laser reflecting pyrite framboids, with some red-shifted reflection from pyrite slightly below surface. CLSM photomicrographs captured with oil objective 63× and 1.40 NA by

application of Ar and HeNe-lasers (excitation with 458 nm, 496 nm and 633 nm laser lines; voxel-width: A: 50.4 nm; B: 121.8 nm; C: 240.5 nm; D: 113.7 nm; scan format 1024×1024 pixel; digital zoom at 2.4, bidirectional scanning).

In contrast to the identified sporinite(?) in images by Czaja (**Fig. 8**), the sporinite in the work by Kus is interpreted to have red-shifted and lower fluorescence intensity emission compared to telalginite (**Fig. 10A, C**). Also identified in the images by Kus is the presence of non-fluorescent coccospheres (**Fig. 10D**), as documented by previous workers [22, 23]. Some diagenetic pyritization of individual coccospheres is evident as blue reflections from sulfide (**Fig. 11A, B**). Fluorescence imaging of bituminite from approximately 1.5 µm below the sample surface (**Fig. 11C**) shows a discrete red-shift in emission compared to the sample surface. Reflection (not autofluorescence) from subsurface sulfide framboids also shows red-shift with greater frequency of green (as opposed to blue) light imaged (**Fig. 11C**), possibly because more of the emitted photon energy is lost to frictional interaction as it passes through the sample. The fluorescence red-shift of bituminite and reflectance red-shift of pyrite can be visually compared between **Figure 11C,** where AOM and pyrite below the sample surface are red-shifted, and **Figure 11D,** where AOM in the sample surface is relatively blue-shifted, and some pyrite just below the sample surface reflects in green wavelengths compared to blue reflections at the sample surface.

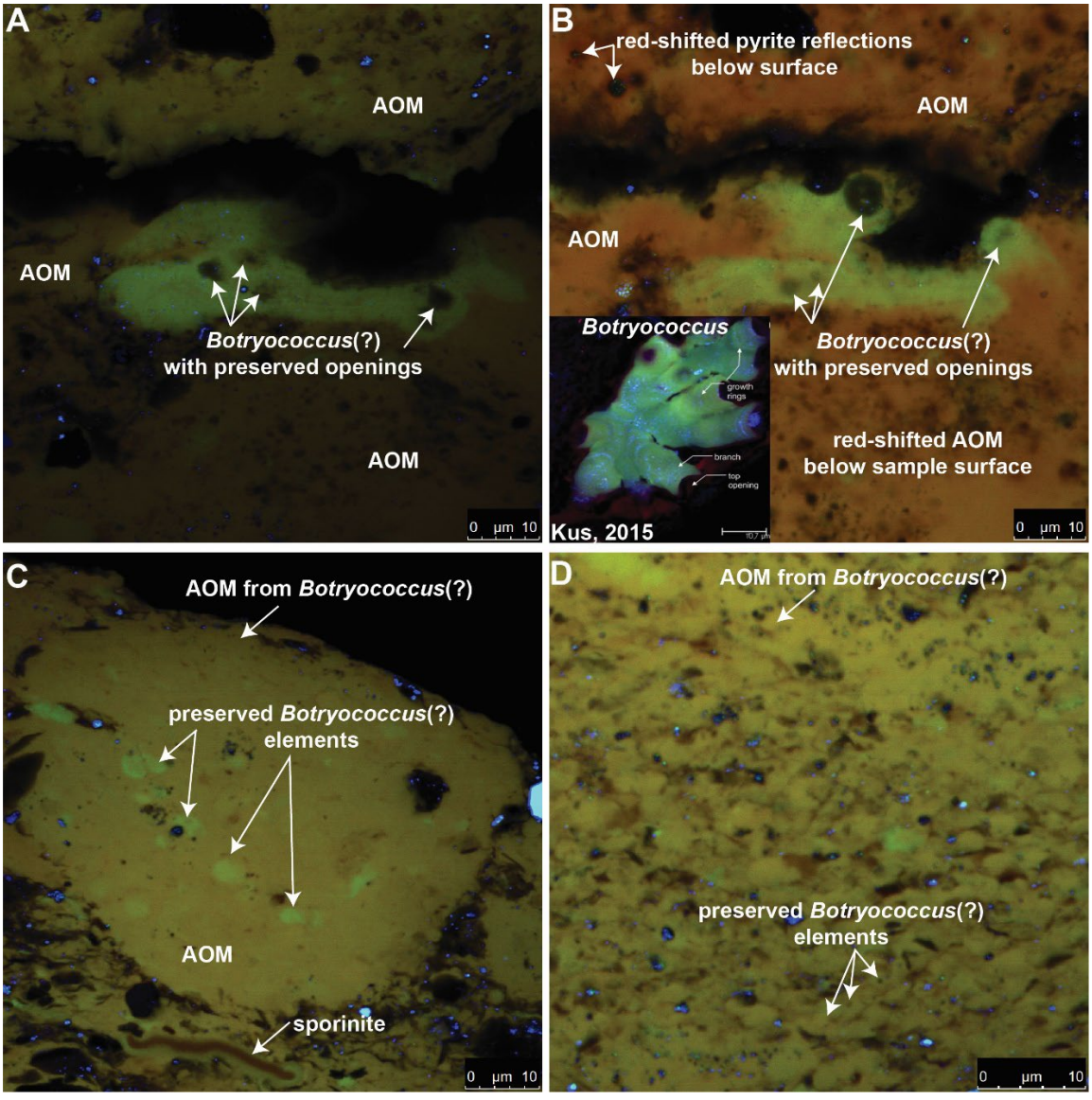

Figure 12. Confocal laser scanning microscopy (CLSM) photomicrographs of KC-1 sample from CLSM WG co-convener Jolanta Kus. **A**. *Botryococcus*(?) with preserved openings. **B**. Same field as A but from 2-3 µm below the sample surface showing red-shifted amorphous organic matter (AOM) fluorescence and pyrite reflection. **C-D**. AOM with some preserved *Botryococcus*(?) elements. CLSM photomicrographs captured with 63× oil objective (1.40 NA) by application of Ar and HeNe-lasers (excitation with 458 nm, 496 nm, and 633 nm laser lines; voxel-width: A: 73.0 nm; B: 73.0 nm; C: 70.3 nm; D: 48.2 nm; scan format 1024×1024 pixel; digital zoom at 2.4, bidirectional scanning).

An important observation in the imaging by Kus is the presence of organic matter with morphology suggestive of remnants of *Botryococcus* (**Fig. 11A**), a freshwater [24-26] to brackish, moderate-salinity green alga. The living form of *Botryococcus braunii* has been reported to occur in fresh water as well as in saltwater conditions [27]. The interpreted presence of a moderate-salinity alga in the marine [28-30] Kimmeridge Clay Formation is contradictory and, if correct, implies proximal deposition, such as an estuarine setting, where transported moderate-salinity algae may have accumulated. Nevertheless, the morphological preservation of *Botryococcus*-like organic matter is well-documented in **Figure 12A-B**, including an example of unambiguous *Botryococcus* (from Visean lignite, Russia [5]) for comparison in the inset of **Figure 12B**. The visual similarities of branches and top and side openings is quite striking. **Figure 12A-B** also provide comparison of the sample surface (**Fig. 12A**) and a focal plane from 2-3 µm below the surface (**Fig. 12B**), allowing further visual confirmation of fluorescence red-shift from AOM below the surface and reflectance red-shift from pyrite below the surface. If the interpretation of preserved *Botryococcus* morphology is correct, it suggests that transitional states between remnant *Botryococcus* and unfigured AOM also may be present, which is suggested in **Figure 12C-D**, where preserved mottled structures and blue-shifted areas may be poorly preserved remnants of individual *Botryococcus* branches.

CLSM imaging and spectroscopy of the KC-1 sample by Angeles Borrego (INCAR) employed a Leica SP8 confocal system on a Leica DMi8 microscope. Using the 405 nm diode laser, fluorescence emission spectroscopy of an AOM fragment (**Fig. 13A**) indicated the wavelength of maximum emission (λ_{max}) was approximately 562 nm (**Fig. 13B**). This value converts to an equivalent BR_o value of 0.52% using the empirical calibration of Hackley and Kus [1], which is significantly higher than either of the measured BR_o or VR_o values reported above (0.29% and 0.42%, respectively). However, the calibration equation of Hackley and Kus [1] was determined for *Tasmanites* telalginite and solid bitumen in Devonian shale of the Appalachian Basin, which is a significantly different maceral type and geologic age than the Jurassic sample considered herein. Using an empirical calibration ($BR_o = 0.0025*\lambda_{max}-1.1168$), derived from data in Stasiuk [31] for stromatolitic *Gloeocapsomorpha prisca* (*G. prisca*) alginite and co-occurring solid bitumen, results in a calculated BR_o value of 0.29%, matching the measured value. However, spectra collected from within another AOM fragment (**Fig. 13C-D**) showed a substantial range in λ_{max} with values of approximately 562 nm (location 1), 523 nm (2), 534 nm (3), and 516 nm (4). These data show little variability in emission intensity and were therefore considered on average (avg. of 539 nm, n=5). This value converts to a BR_o value of 0.21% using the empirical calibration from Stasiuk [31], which is lower than the measured value (0.29%), but closer than the value calculated by the application of the Hackley and Kus [1] calibration (0.45%). The closer correspondence of calculated BR_o values using data from stromatolitic *G. prisca* suggest misapplication of the Hackley and Kus [1] calibration from *Tasmanites*.

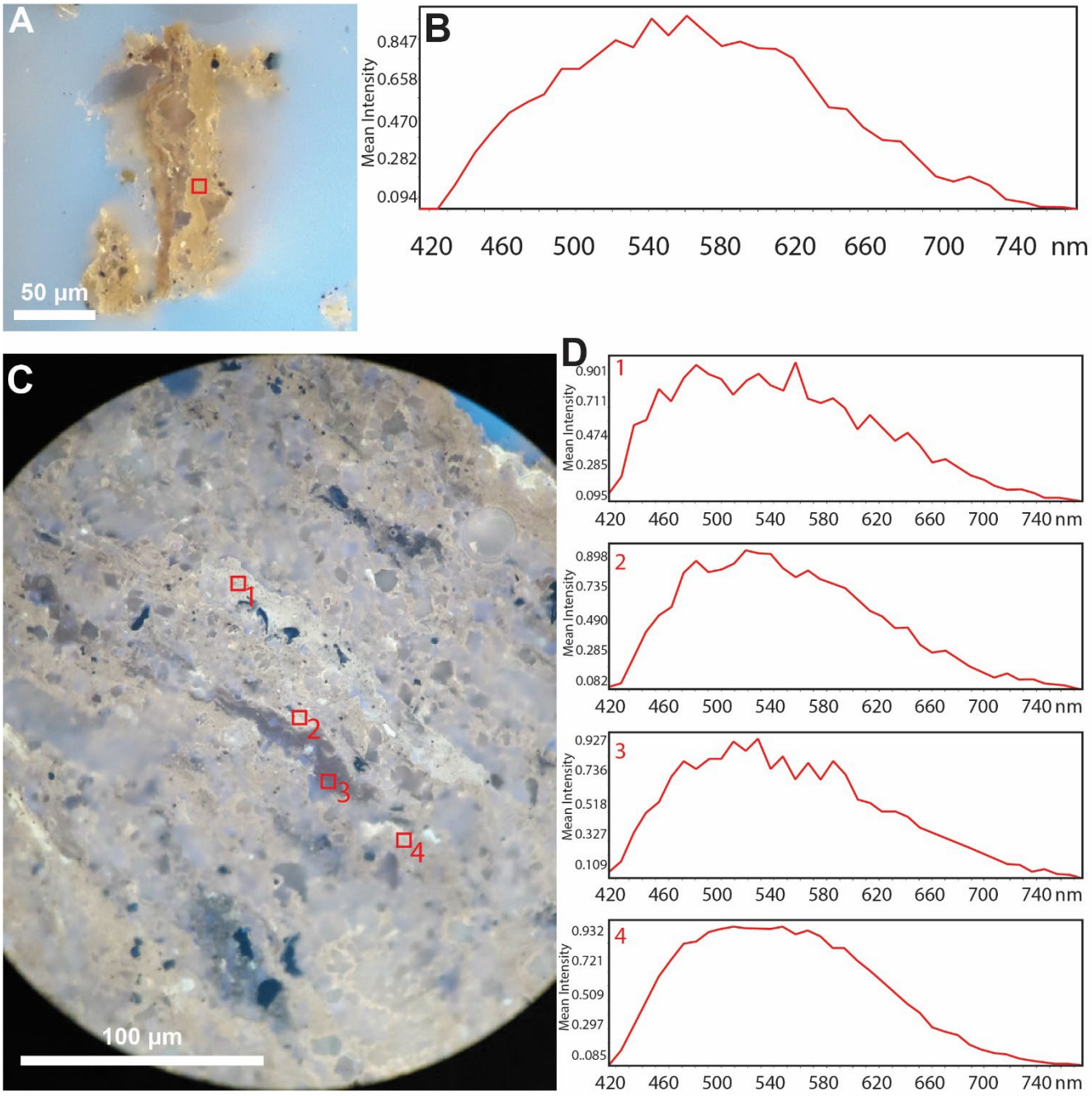

Figure 13. Confocal laser scanning microscopy (CLSM) spectroscopy data from KC-1 sample contributed from CLSM WG participant Angeles Borrego. **A**. Fluorescence image of amorphous organic matter (AOM) embedded in blue fluorescing epoxy-resin. **B**. Emission spectrum from region of interest shown by red box in A. **C**. Fluorescence image of a second AOM fragment, with four locations of spectral data collection annotated. **D**. Spectra from four locations marked in C.

Efforts to acquire 3-D CLSM imaging of the KC-1 sample by Hackley resulted in unintentional photo-oxidation of the sample surface, that is, a positive alteration [32-34], causing an increase in fluorescence emission intensity in an area of prolonged (14 min, 13 sec) laser exposure (**Figure 14**).

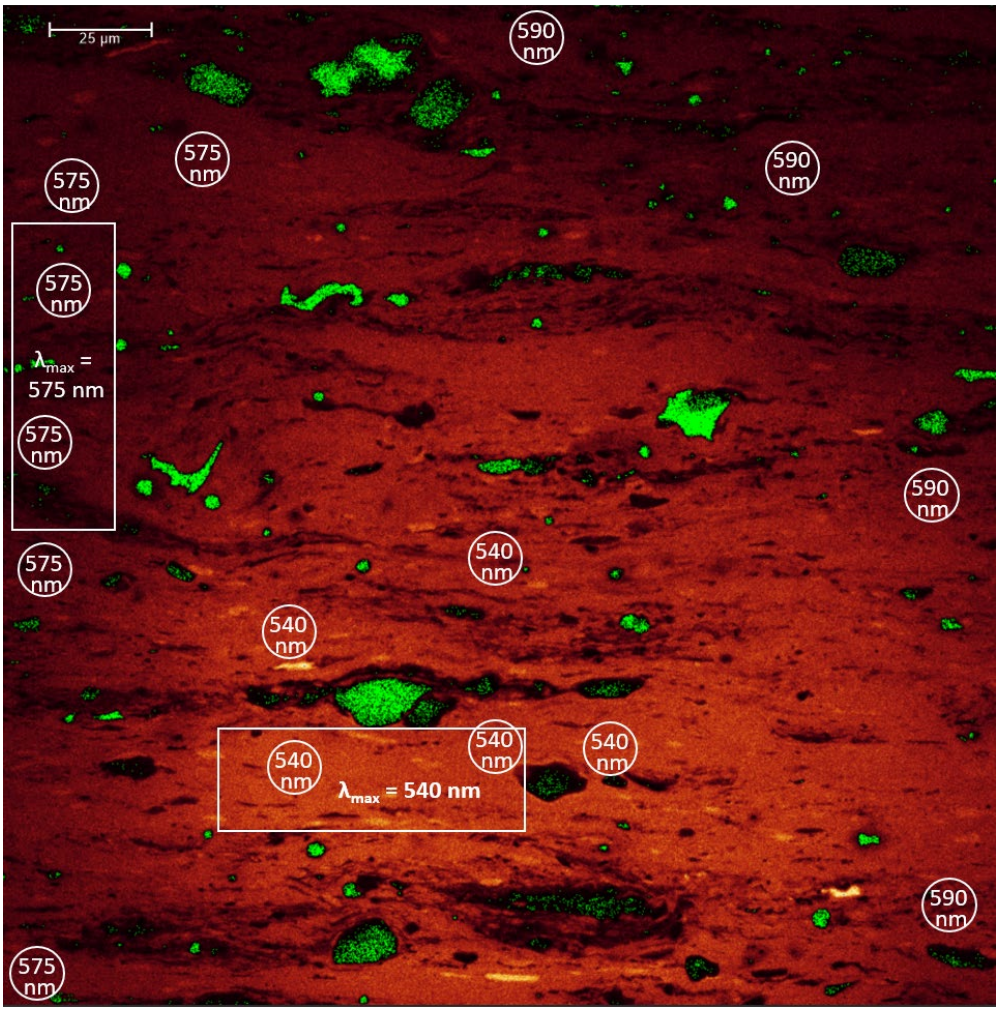

Figure 14. CLSM spectroscopy data from KC-1 sample contributed from Hackley. Rectangular and circular regions of interest (ROI) are labeled with average λ_{max} values from all pixels in the ROI. Note the area of significant positive alteration (higher emission intensity) in the lower center of the field and the blue shifted fluorescence in the area of higher emission intensity.

The unintentional fluorescence alteration provided an opportunity to compare its effect on fluorescence emission to adjacent unaffected areas. In addition to the obvious increase in emission intensity, an immediate observation is the blue-shift in wavelengths of fluorescence emission where photo-oxidation occurred. A large (~1600 µm^2) rectangular ROI shows average λ_{max} of 575 nm in an unaltered area, whereas average λ_{max} is blue-shifted to 540 nm in a similarly sized and shaped ROI in the adjacent area of photo-oxidation. This observation holds whether small or large ROIs are used for analysis. **Figure 14** also shows 10 circular ROIs of (~160 µm^2 each) within the unaltered area with average λ_{max} of 575-590 nm, whereas five circular ROIs (~160 µm^2) in the area of photo-oxidation have average λ_{max} of 540 nm. Within both the photo-oxidized and unaltered zones the fluorescence emission is blue-shifted in higher emission intensity areas relative to areas with lower emission intensity (**Figure 15**), suggesting a compositional difference perhaps equivalent to the relative degradation for algal elements discussed above in the imaging work by Kus. The λ_{max} is 585 nm in unaltered areas, which does not correspond to the average λ_{max} measured by Borrego of ~539 nm, possibly indicating the occurrence of stray light from the blue fluorescing epoxy in the kerogen concentrate, or the need for standardization in fluorescence spectroscopy, despite the fact that both data sets were collected using a 405 nm diode laser.

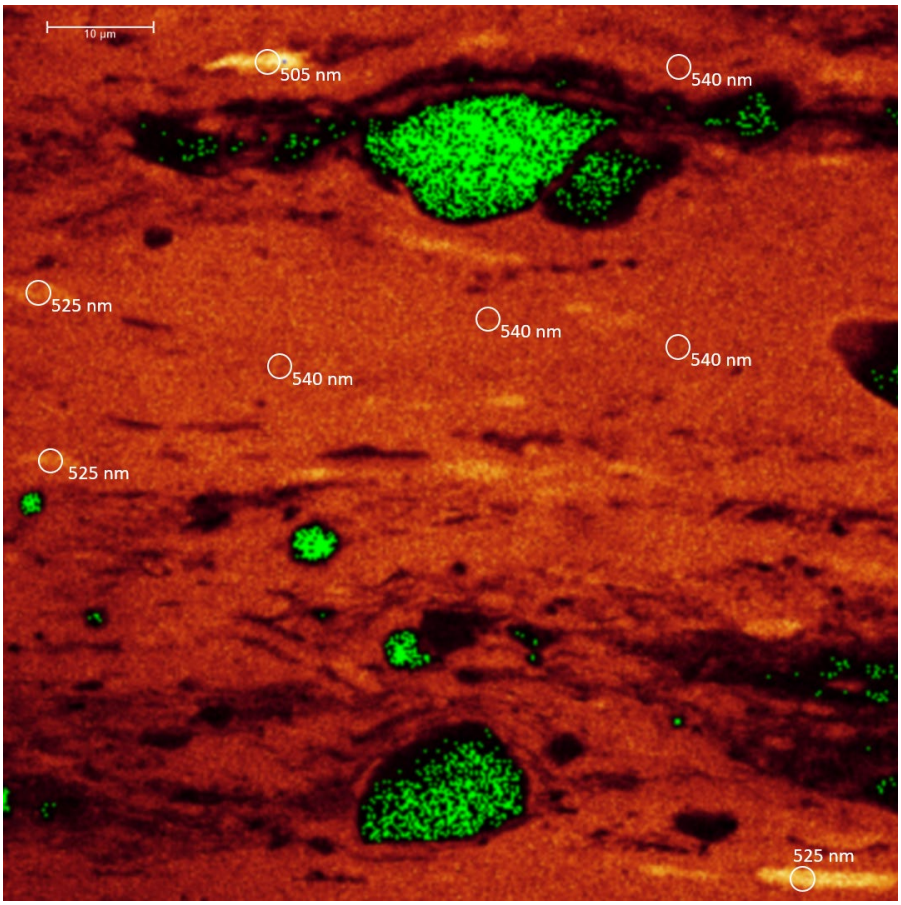

Figure 15. Photo-oxidized region from center of Figure 12. Note blue-shift in emission from areas of higher emission intensity.

CLSM fluorescence spectroscopy by Kus took a different approach, wherein three laser lines were used (458 nm, 496 nm, and 633 nm) and the response from all three was evaluated together over the emission range of 457 to 800 nm. Ten locations were selected for measurement and averaged together, allowing for the estimation of standard deviation of measurement as shown by error bars in **Figure 16**. One important artifact from this approach is the increased red response due to application of the 633 nm laser, as noted in previous work [6]. Nevertheless, the λ_{max} value of 562 nm reported by Kus is similar to the value reported by Hackley (575 nm) and converts to a calculated BR_o value of 0.29% (using the Stasiuk calibration), matching the measured value.

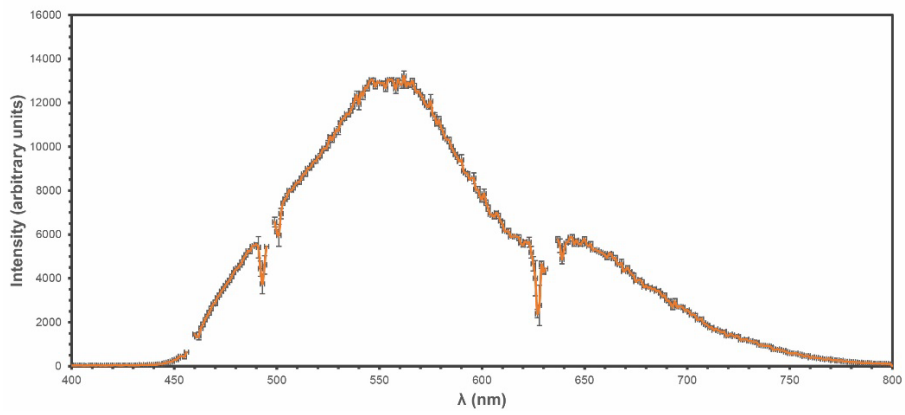

Figure 16. Emission spectra reported by Kus using 10 measurement locations and three laser lines.

Future directions of the working group

As reported above, there is no current interest from WG participants in continuing the activities as a joint project. Therefore, the working group is hereby closed, and the conveners will revert to a collaborative relationship. This report represents the final product of the CLSM WG, although it may be condensed and submitted for publication in a future peer-reviewed manuscript. A notice will be posted in *ICCP News* regarding the cessation of the WG activities.

The conveners (Hackley and Kus) will monitor future interest and activity in the organic petrology community using CLSM and, if warranted, future reactivation of the WG will be considered. As a matter of consideration for other conveners of working groups in ICCP, the lack of interest for continuation of the CLSM WG was judged to be due to several factors: changing jobs and retirement of WG members; global lockdown and resultant laboratory access restrictions from the COVID-19 pandemic; and insufficient leadership and direction from the WG conveners. For example, to this last point, no specific instructions were provided for CLSM analysis of the KC sample because of the diverse interests and research directions of the WG members. A future iteration of this WG, or other WGs in ICCP, should provide explicit instructions for sample analysis, and should be persistent through regular requests for participatory results.

Summary

The confocal laser scanning microscopy (CLSM) working group (WG) of the ICCP was open from 2015 to 2021, during which several WG members jointly analyzed an organic-rich, immature sample from the Kimmeridge Clay Formation (sample ID KC-1). As part of the WG investigation, the KC-1 sample was processed into polished whole rock pellets, polished kerogen concentrate pellets, and strew slides. Atomic force microscopy evaluation of a mechanically polished sample and a correlative location after polishing by broad ion beam (BIB), indicated that increased surface flattening was caused by ion milling, which resulted in higher reflectance of amorphous organic matter (AOM). Conversely, exposure by ion milling of nano-sulfides embedded in the AOM resulted in overall decreased surface flatness in non-correlative locations. The magnitude of surface deviation from perfect flatness was dependent on the scale of observation and highlights our continued need for research in BIB milling effects to sedimentary organic matter. Findings from CLSM imaging included the interpreted presence of *Botryococcus* and incomplete blocking of laser light from highly reflective sulfides and fusinite. Radiation halos of decreased fluorescence intensity around radioactive minerals were noted in conventional and CLSM imaging and interpreted as due to substitution of U for Fe in sulfides. Three-dimensional CLSM imaging also noted a red-shift of reflectance and auto-fluorescence from below the sample surface. CLSM fluorescence spectroscopy was used to investigate a blue-shift from positive alteration due to laser-induced photo-oxidation of the sample surface. Fluorescence blue-shift also was associated to higher fluorescence intensity regions in AOM, probably due to differences in composition. Differences in procedures for spectroscopic data collection and reported results highlight the need for fluorescence spectroscopy standardization as applied via CLSM. Last, the suitability of CLSM to predict solid bitumen reflectance via calibration to an extant data set shows further viability of this tool as a petrographic thermal probe of low maturity sedimentary organic matter.

Acknowledgements

Reviews of this report by Celeste Lohr and Maggie Sanders (U.S. Geological Survey) improved its quality and clarity. The conveners of the ICCP CLSM WG are indebted to the participants in the WG for their individual contributions. Gilbert Min and Michael Saba (Keysight Technologies, Inc.) provided AFM analyses. Javin Hatcherian and Brett Valentine (U.S. Geological Survey) provided sample preparation. Jing-Jiang Yu and William Podrazky (Hitachi High Technologies America, Inc.) supervised AFM analyses and provided BIB-milling,

respectively. Amy Beaven (Univ. of Maryland) supervised CLSM analyses. Any use of trade, firm, or product names is for descriptive purposes only and does not imply endorsement by the U.S. Government.

References

[1] Hackley PC, Kus J. Thermal maturity of *Tasmanites* microfossils from confocal laser scanning fluorescence microscopy. Fuel 2015;143:343-50.

[2] Kus J, Hackley PC, Ostertag-Henning C. Confocal laser scanning microscopy (CLSM) applied to microstructural analysis of Tasmanites in the Huron Member of the Ohio Shale, Appalachian Basin, USA. *Schriftenreihe der Deutschen Gesellschaft für Geowissenschaften, 80, Abstracts of Lectures and Posters GeoHannover 2012 - GeoRohstoffe für das 21.* Jahrhundert; 2012:432.

[3] Hackley PC, Burruss RC, Boyd J. Application of excitation-emission fluorescence microscopy to thermal maturity of geological samples. *Geological Society of America.* 45. Denver, Colorado; 2013:650.

[4] Hackley PC, Burruss RC. Fluorescence spectroscopy of Tasmanites microfossils in relation to chemical composition: application of confocal laser scanning microscopy. *Geological Society of America.* 47. Baltimore, MD; 2015:456.

[5] Kus J. Application of confocal laser-scanning microscopy (CLSM) to autofluorescent organic and mineral matter in peat, coals and siliciclastic sedimentary rocks — A qualitative approach. International Journal of Coal Geology 2015;137:1-18.

[6] Hackley PC, Jubb AM, Burruss RC, Beaven AE. Fluorescence spectroscopy of ancient sedimentary organic matter via confocal laser scanning microscopy (CLSM). International Journal of Coal Geology 2020;223:103445.

[7] Hackley PC, Valentine BJ, Hatcherian JJ. On the petrographic distinction of bituminite from solid bitumen in immature to early mature source rocks. International Journal of Coal Geology 2018;196:232-45.

[8] Valentine BJ, Hackley PC, Hatcherian J, Yu J-J. Reflectance increase from broad beam ion milling of coals and organic-rich shales due to increased surface flatness. International Journal of Coal Geology 2019;201:86-101.

[9] Bolin TB, Birdwell JE, Lewan MD, Hill RJ, Grayson MB, Mitra-Kirtley S, et al. Sulfur species in source rock bitumen before and after hydrous pyrolysis determined by x-ray absorption near-edge structure. Energy & Fuels 2016;30(8):6264-70.

[10] Birdwell JE, Washburn KE. Rapid analysis of kerogen hydrogen-to-carbon ratios in shale and mudrocks by laser-induced breakdown spectroscopy. Energy & Fuels 2015;29(11):6999-7004.

[11] Hackley PC, Dennen KO, Garza D, Lohr CD, Valentine BJ, Hatcherian JJ, et al. Oil-source rock correlation studies in the unconventional Upper Cretaceous Tuscaloosa marine shale (TMS) petroleum system, Mississippi and Louisiana, USA. Journal of Petroleum Science and Engineering 2020;190:107015.

[12] Pickel W, Kus J, Flores D, Kalaitzidis S, Christanis K, Cardott BJ, et al. Classification of liptinite – ICCP System 1994. International Journal of Coal Geology 2017;169:40-61.

[13] Teichmüller M. Über neue Macerale der Liptinit-Gruppe und die Entstehung des Micrinits. Fortschr Geol Rheinl Westfalen 1974;24:37-64.

[14] Faraj BSM, Mackinnon IDR. Micrinite in southern hemisphere subbituminous and bituminous coals: redefined as fine grained kaolinite. Organic Geochemistry 1993;20(6):823-41.

[15] Machovic V, Havelcova M, Sykorova I, Borecka L, Lapcak L, Mizera J, et al. Raman mapping of coal halos induced by uranium mineral radiation. Spectrochim Acta A Mol Biomol Spectrosc 2021;246:118996.

[16] Luo Q, Zhong N, Qin J, Li K, Zhang Y, Wang Y, et al. Thucholite in Mesoproterozoic shales from northern north China: Occurrence and indication for thermal maturity. International Journal of Coal Geology 2014;125:1-9.

[17] ISO. 25178-2 Geometric product specifications (GPS) - surface texture, areal: Part 2, terms, definitions and surface texture parameters. ISO; 2012:47.

[18] Gadelmawla ES, Koura MM, Maksoud TMA, Elewa IM, Soliman HH. Roughness parameters. Journal of Materials Processing Technology 2002;123:133-45.
[19] Grobe A, Schmatz J, Littke R, Klaver J, Urai JL. Enhanced surface flatness of vitrinite particles by broad ion beam polishing and implications for reflectance measurements. International Journal of Coal Geology 2017;180:113-21.
[20] Hackley PC, Jubb AM, Valentine BJ, Hatcherian JJ, Yu J-J, Podrazky WK. Investigating the effects of broad ion beam milling to sedimentary organic matter: surface flattening or heat-induced aromatization and condensation? Fuel 2020;282(118627).
[21] ICCP. The new inertinite classification (ICCP System 1994). Fuel 2001;80:459-71.
[22] Lees JA, Bown PR, Young JR. Photic zone palaeoenvironments of the Kimmeridge Clay Formation (Upper Jurassic, UK) suggested by calcareous nannoplankton palaeoecology. Palaeogeography, Palaeoclimatology, Palaeoecology 2006;235(1-3):110-34.
[23] Lees JA, Bown PR, Young JR, Riding JB. Evidence for annual records of phytoplankton productivity in the Kimmeridge Clay Formation coccolith stone bands (Upper Jurassic, Dorset, UK). Marine Micropaleontology 2004;52(1-4):29-49.
[24] Rao AR, Dayananda C, Sarada R, Shamala TR, Ravishankar GA. Effect of salinity on growth of green alga *Botryococcus braunii* and its constituents. Bioresour Technol 2007;98(3):560-4.
[25] Metzger P, Largeau C. *Botryococcus braunii*: a rich source for hydrocarbons and related ether lipids. Appl Microbiol Biotechnol 2005;66(5):486-96.
[26] Vandenbroucke M, Largeau C. Kerogen origin, evolution and structure. Organic Geochemistry 2007;38(5):719-833.
[27] Masters MJ. The occurrence of *Chytridium marylandicum* on *Botryococcus braunii* in School Bay of the Delta Marsh. Canadian Journal of Botany 1971;49:1479-85.
[28] Boussafir M, Gelin F, Lallier-Vergès E, Derenne S, Bertrand P, Largeau C. Electron microscopy and pyrolysis of kerogens from the Kimmeridge Clay Formation, UK: source organisms, preservation processes, and origin of microcycles. Geochimica et Cosmochimica Acta 1995;59(18):3731-47.
[29] Fishman NS, Hackley PC, Lowers HA, Hill RJ, Egenhoff SO, Eberl DD, et al. The nature of porosity in organic-rich mudstones of the Upper Jurassic Kimmeridge Clay Formation, North Sea, offshore United Kingdom. International Journal of Coal Geology 2012;103:32-50.
[30] Tribovillard N-P, Desprairies A, Lallier-Vergès E, Bertrand P, Moureau N, Ramdani A, et al. Geochemical study of organic-matter rich cycles from the Kimmeridge Clay Formation of Yorkshire (UK): productivity versus anoxia. Palaeogeography, Palaeoclimatology, Palaeoecology 1994;106:165-81.
[31] Stasiuk LD. Fluorescence properties of Palaeozoic oil-prone alginite in relation to hydrocarbon generation, Williston Basin, Saskatchewan, Canada. Marine and Petroleum Geology 1994;11:219-31.
[32] Ottenjann K. Fluorescence alteration and its value for studies of maturation and bituminization. Organic Geochemistry 1988;12(4):309-21.
[33] Davis A, Rathbone RF, Lin R, Quick JC. Observations concerning the nature of maceral fluorescence alteration with time. Organic Geochemistry 1990;16(4-6):897-906.
[34] Pradier B, Landais P, Rochdi A, Davis A. Chemical basis of fluorescence alteration of crude oils and kerogens ll. Fluorescence and infrared micro-spectrometric analysis of vitrinite and liptinite. Organic Geochemistry 1992;18(3):241-8.